

Article

# Crystal Structures of New Ivermectin Pseudopolymorphs

Kirill Shubin <sup>1</sup>, Agris Bērziņš <sup>2</sup> and Sergey Belyakov <sup>1,\*</sup>

<sup>1</sup> Latvian Institute of Organic Synthesis, 21 Aizkraukles St., LV-1006 Riga, Latvia; kir101@osi.lv

<sup>2</sup> Faculty of Chemistry, University of Latvia, 1 Jelgavas St., LV-1004 Riga, Latvia; agris.berzins@lu.lv

\* Correspondence: serg@osi.lv; Tel.: +371-67014897

**Abstract:** New pseudopolymorphs of ivermectin (IVM), a potential anti-COVID-19 drug, were prepared. The crystal structure for three pseudopolymorphic crystalline forms of IVM has been determined using single-crystal X-ray crystallographic analysis. The molecular conformation of IVM in crystals has been compared with the conformation of isolated molecules modeled by DFT calculations. In a solvent with relatively small molecules (ethanol), IVM forms monoclinic crystal structure (space group  $I2$ ), which contains two types of voids. When crystallized from solvents with larger molecules, like  $\gamma$ -valerolactone (GVL) and methyl *tert*-butyl ether (MTBE), IVM forms orthorhombic crystal structure (space group  $P2_12_12_1$ ). Calculations of the lattice energy indicate that interactions between IVM and solvents play a minor role; the main contribution to energy is made by the interactions between the molecules of IVM itself, which form a framework in the crystal structure. Interactions between IVM and molecules of solvents were evaluated using Hirshfeld surface analysis. Thermal analysis of the new pseudopolymorphs of IVM was performed by differential scanning calorimetry and thermogravimetric analysis.

**Keywords:** ivermectin; pseudopolymorph; crystal structure analysis; Hirshfeld surface analysis



**Citation:** Shubin, K.; Bērziņš, A.; Belyakov, S. Crystal Structures of New Ivermectin Pseudopolymorphs. *Crystals* **2021**, *11*, 172. <https://doi.org/10.3390/cryst11020172>

Academic Editor: Alexander Pöthig  
Received: 14 January 2021  
Accepted: 30 January 2021  
Published: 9 February 2021

**Publisher's Note:** MDPI stays neutral with regard to jurisdictional claims in published maps and institutional affiliations.



**Copyright:** © 2021 by the authors. Licensee MDPI, Basel, Switzerland. This article is an open access article distributed under the terms and conditions of the Creative Commons Attribution (CC BY) license (<https://creativecommons.org/licenses/by/4.0/>).

## 1. Introduction

Ivermectin (IVM) is a macrocyclic lactone developed in the 1980s as an antiparasitic multitarget drug with nematocidal, acaricidal and insecticidal activities [1,2]. It is a semisynthetic substance, which is used as a mixture of two components: major B<sub>1a</sub> (R = Et) and minor B<sub>1b</sub> (R = Me), as shown in Figure 1.

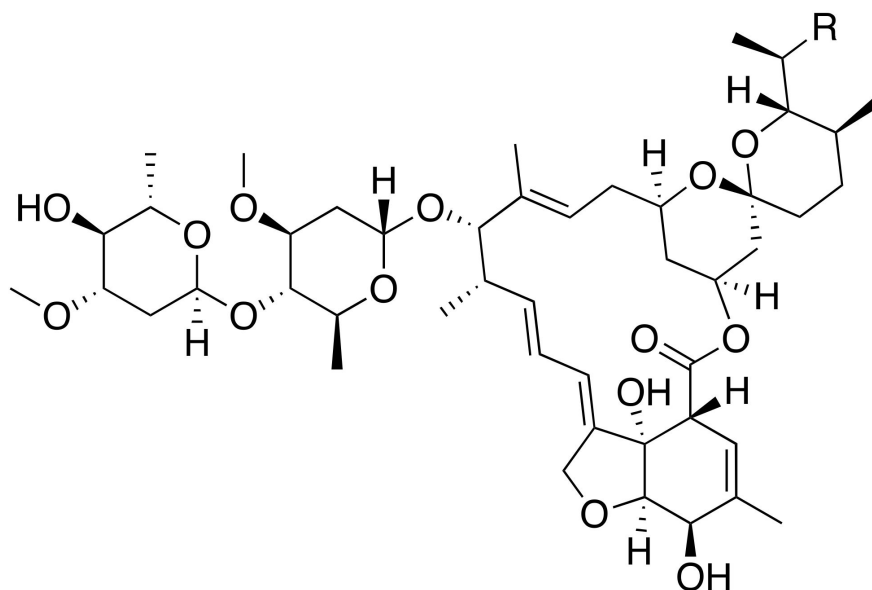


**Figure 1.** Ivermectin as a mixture of two components B<sub>1a</sub> (R = Et) and B<sub>1b</sub> (R = Me).

Currently hundreds of millions of people are using IVM for treatment of various parasitic diseases, including onchocerciasis, lymphatic filariasis, scabies, etc. [3]. While at nanomolar concentrations it is effective mostly against nematodes, at higher concentrations, multiple new targets were identified [4,5]. Activity against various types of cancer has been reported [6–9]. IVM is an approved drug for treatment of rosacea due to its antiparasitic properties complemented by anti-inflammatory activity [10–12]. In addition, the activity of IVM against various viruses [13], including COVID-19 [14,15], is of a special interest. Several clinical studies are planned or have been started for this indication [16,17].

Nature and properties of a solid form of drugs is important for their production and all relevant applications [18]. Analysis and understanding of the internal molecular arrangements in crystalline materials bear the key to preparation of materials with controllable and predictable solubility, hygroscopicity and mechanical properties [19,20].

Interestingly, only few crystalline structures of IVM have been reported so far. First, two single-crystal diffraction data sets on a close analogue avermectin are deposited in the Cambridge Crystallographic Data Centre with CCDC refcodes BASVAS [21] and YOCYAT [22]. IVM was discussed in a context of interaction with the transmembrane domain of certain receptors using models with low resolution [23,24]. Additionally, several crystalline polymorphs were characterized by powder X-ray diffraction [25–28]. The only single crystal data of IVM B<sub>1a</sub> published to date was reported by Seppala et al.: CSD, Version 5.40, November 2019; CCDC refcode BIFYOF [29]. The IVM crystal structure represents monoclinic modification (space group *I*2) of IVM as acetone-chloroform solvate. This form is not satisfactory for drug application due to the presence of a toxic chlorinated solvent (chloroform).

In this study, we performed crystallization of IVM from several solvents to investigate whether other crystal structures of this compound can be obtained. It was found that new pseudopolymorphs, isomorphic to the already reported monoclinic structure, contain various solvent molecules in the structure cavities. Moreover, in the presence of larger solvent molecules, orthorhombic structure can be also obtained having bigger cavities able to accommodate larger solvent molecules. Both types of crystal structures were analyzed and compared by characterizing intermolecular interactions and molecular conformation, and the ability of IVM to incorporate different solvents is discussed.

## 2. Materials and Methods

### 2.1. Synthesis of Ivermectin Pseudopolymorphs

IVM was obtained from Key Organics,  $\gamma$ -valerolactone (GVL) from Carbosynth, UK. New pseudopolymorphs of IVM were prepared by crystallization of the starting material from an appropriate solvent. Preparation of IVM as ethanol solvate (I) was carried out by dissolution of IVM (1 g) in EtOH (5 mL) at reflux. Solution was cooled to room temperature and left for 48 h to effect the crystallization. Crystals of IVM as GVL solvate (II) were prepared by brief heating of IVM (1 g) in GVL (3 mL) up to 120 °C, and the obtained clear solution was left at room temperature for 72 h to effect the crystallization. Pseudopolymorph of IVM as methyl *tert*-butyl ether (MTBE) solvate (III) was prepared by dissolution of IVM (1 g) in MTBE (20 mL) at reflux and addition of hexanes (20 mL). Crystals were obtained at room temperature in 24 h.

### 2.2. Single Crystal X-ray Diffraction

For compounds I (ethanol solvate), II (GVL solvate) and III (MTBE solvate) diffraction data were collected at low temperature on a Rigaku, XtaLAB Synergy, Dualflex, HyPix (Rigaku Corporation, Tokyo, Japan) diffractometer using copper monochromated Cu-K $\alpha$  radiation ( $\lambda = 1.54184 \text{ \AA}$ ). The crystal structures were solved by direct methods with the ShelXT (Version 2014/5, Georg-August Universität Göttingen, Germany) [30] structure solution program using intrinsic phasing and refined with the SHELXL (version 2016/6, Georg-August Universität Göttingen, Germany) refinement package [31]. All calculations were performed with the help of Olex2 software (version Olex2.refine,

Durham University, UK) [32]. The lattice parameters for solvate I were determined also at room temperature; the density of the compound was measured by the flotation method in ethanol-chloroform system. For calculation of the density, the actual composition of crystal I is  $2(\text{IVM}) \times 2\text{C}_2\text{H}_5\text{OH} \times 1.5\text{H}_2\text{O}$  (with  $Z = 2$ ), where  $\text{IVM} = 0.8\text{B}_{1a} \times 0.2\text{B}_{1b}$ , where  $\text{B}_{1a} = \text{C}_{48}\text{H}_{74}\text{O}_{14}$  and  $\text{B}_{1b} = \text{C}_{47}\text{H}_{72}\text{O}_{14}$ . Molecular crystals of bulky molecules with many degrees of freedom, with disordered solvents and not containing heavy atoms (the heaviest atom in IVM is oxygen) cannot be close to ideal, therefore,  $R$ -factors for such crystal structures are quite high. Table 1 lists the main crystal data for these compounds.

**Table 1.** Crystal data and structure refinement parameters for solvates I, II and III <sup>1</sup>.

Parameter	I at Low Temperature	I at Room Temperature	II	III
Empirical formula	(IVM) × C <sub>2</sub> H <sub>5</sub> OH × 0.75H <sub>2</sub> O	(IVM) × C <sub>2</sub> H <sub>5</sub> OH × 0.75H <sub>2</sub> O	2(IVM) × 0.5C <sub>5</sub> H <sub>8</sub> O <sub>2</sub>	2(IVM) × 0.5C <sub>5</sub> H <sub>12</sub> O
Formula weight	931.85	931.85	1794.59	1787.605
Temperature (K)	173	293	160	160
Crystal size (mm <sup>3</sup> )	0.21 × 0.11 × 0.08	0.17 × 0.09 × 0.06	0.22 × 0.16 × 0.11	0.21 × 0.17 × 0.12
Crystal system	Monoclinic	Monoclinic	Orthorhombic	Orthorhombic
Space group	<i>I</i> 2	<i>I</i> 2	<i>P</i> 2 <sub>1</sub> 2 <sub>1</sub> 2 <sub>1</sub>	<i>P</i> 2 <sub>1</sub> 2 <sub>1</sub> 2 <sub>1</sub>
<i>a</i> (Å)	14.8197(7)	14.8612(9)	16.7127(2)	16.7309(1)
<i>b</i> (Å)	9.1753(5)	9.1973(6)	24.5777(2)	24.5805(2)
<i>c</i> (Å)	39.094(2)	39.201(4)	24.5908(2)	24.5797(2)
β (°)	94.490(5)	95.04(5)	90.0	90.0
Unit cell volume (Å <sup>3</sup> )	5299.5(5)	5337.4(7)	10100.9(2)	10108.5(1)
Molecular multiplicity	4	4	4	4
Calculated density (g/cm <sup>3</sup> )	1.168	1.161	1.180	1.175
Measured density (g/cm <sup>3</sup> )		1.16		
Absorption coefficient (mm <sup>-1</sup> )	0.703	0.698	0.702	0.696
<i>F</i> (000)	2023.5	2023.5	3887.2	3875.2
2θmax (°)	156.0	150.0	155.0	155.0
Reflections collected	29158	5217	71647	75795
Number of independent reflections	9710	-	20489	20330
Reflections with <i>I</i> > 2σ( <i>I</i> )	9485	-	18694	19029
Number of refined parameters	601	-	1143	1143
<i>R</i> -factors (for <i>I</i> > 2σ( <i>I</i> ) and for all data)	0.0971, 0.0982	-	0.0981, 0.1051	0.0972, 0.1010

$$^1 \text{IVM} = 0.8(\text{C}_{48}\text{H}_{74}\text{O}_{14}) \times 0.2(\text{C}_{47}\text{H}_{72}\text{O}_{14}).$$

Overlay of IVM geometry was done in BIOVIA Discovery Studio 4.5 Visualizer v4.5.0.15071 (Dassault Systèmes, France), by matching the position of atoms C3, C14 and O26.

### 2.3. Modeling and Quantitative Analysis of Crystal Structures

To better characterize the differences and similarities between the crystal structures of IVM, their Hirshfeld surfaces were generated using CrystalExplorer17 (University of Western Australia, Perth, Australia) [33]. They were analyzed by performing the generation and analysis of Hirshfeld surface 2D fingerprint plots and summarizing the information about intermolecular interactions [34,35]. Additionally, for ethanol solvate I, pairwise intermolecular interaction energies for molecules, for which atoms are within 3.8 Å of the central molecule, were estimated in CrystalExplorer17 at the B3LYP-D2/6-31G(d,p) level [36] with electronic structure calculations performed in Gaussian09.

The gas phase geometry optimizations were carried out using Schrödinger software at the B3LYP/6-311G(d,p) level of theory [37].

#### 2.4. Thermal Analysis

The differential scanning calorimetric/thermogravimetric (DSC/TGA) analysis was performed on a TGA/DSC2 (Mettler Toledo, Greifensee, Switzerland) apparatus. Open 100  $\mu$ L aluminum pans were used. Heating of the samples from 25 to 600  $^{\circ}$ C was performed at a heating rate 10  $^{\circ}$ C $\cdot$ min $^{-1}$ . Samples of 5–10 mg mass were used, and the nitrogen flow rate was 100  $\pm$  10 mL $\cdot$ min $^{-1}$ .

Thermal analysis (TGA and DSC) shows typical data for solid solutions (see files in the Supplementary Materials). The peaks in the DSC patterns, which correspond to the melting process, are quite wide: at 165  $^{\circ}$ C for **I** and at 172  $^{\circ}$ C for **II**. Their half-widths are: 17  $^{\circ}$ C for solvate **I** and 8  $^{\circ}$ C for solvate **II**. Thermal analysis data also show that solvate **II** loses the solvent (GVL) at 83  $^{\circ}$ C. In **I**, this process is not observed. This is due to the fact that solvent in **II** is not stabilized by strong hydrogen bonds.

### 3. Results

#### 3.1. Molecular Structure in the Crystal Cell

For investigation of the molecular structure of IVM by means of X-ray diffraction method, single crystals of **I** have been grown from ethanol solution. It is well known that the semisynthetic substance of IVM represents a mixture of two compounds— $B_{1a}$  and  $B_{1b}$  in molar ratio 80:20. Thus, a solid solution of these two components as a single crystal structure was obtained during crystallization. The formation of solid solutions, where several chemically distinct components occupy the same position in the crystal lattice, is not such a rare occurrence in organic and inorganic chemistry [38]. However, there are not so many crystal structures of this type in crystallographic databases. This is largely due to the technical difficulties observed during their crystallographic studies. Despite the fact that there are two components of IVM in crystals, this paper will further focus on the main component of IVM, namely  $B_{1a}$ . Figure 2 illustrates an Oak Ridge Thermal-Ellipsoid Plot (ORTEP) diagram of solvate **I** showing the atom-labeling scheme and thermal displacement ellipsoids for non-H atoms. For ethyl group (carbon atoms C33 and C34 and hydrogen atoms H33a, H33b, H34a, H34b and H34c), the value of occupancy  $g$ -factor = 0.8 and, for methyl group (carbon atom C33 and hydrogen atoms H33a, H33b and H33c), the value of  $g$ -factor = 0.2.

The major figure of the molecular structure is the 16-membered macrocycle, which consists of atoms C3, C10–C20, O21, C22, C4 and C9. In the crystals, the least-squares plane of this cycle corresponds to the crystallographic plane of (0 3 2). Atoms C15 and C12 have maximal deviations (0.406(5) and  $-0.382(5)$  Å, respectively) from this plane. It should be noted that positive and negative atomic deviations from the plane alternate. Thus, in crystal **I**, the macrocycle has a “crown” conformation. In the fused bicyclic system, both cycles are characterized by an envelope conformation: atom C8 deviates on 0.590(5) Å from the plane of other atoms in the tetrahydrofuran cycle, and atom C9 deviates on 0.627(4) Å from the plane of other five atoms in the cyclohexene cycle. All the other cycles in the molecule have a usual chair conformation.

For the comparison of molecular structures in crystal **I**, in vacuo geometry optimization of the molecule using density functional theory (DFT) calculations was performed. A perspective view of the molecule in the free state and in crystals is shown in Figure 3.

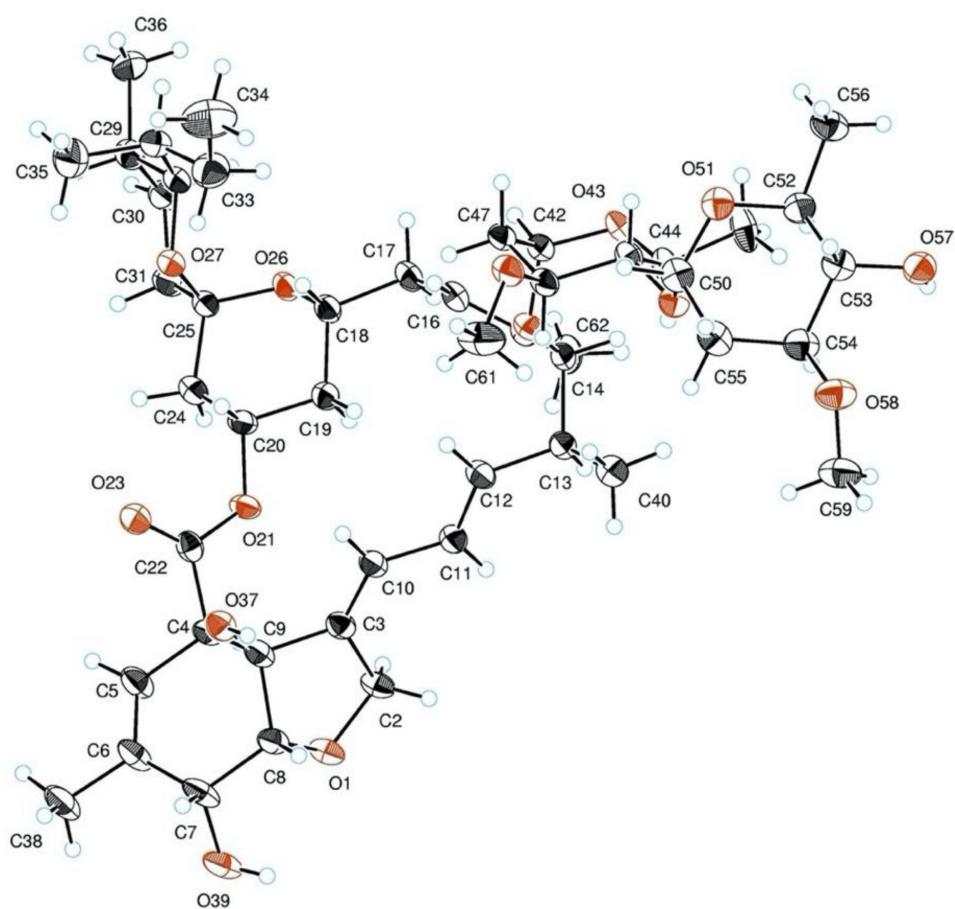


**Figure 2.** ORTEP diagram of IVM molecule in crystal I showing atomic labels and 50% probability displacement ellipsoids. Hydrogen atoms are shown as small spheres of arbitrary radii.

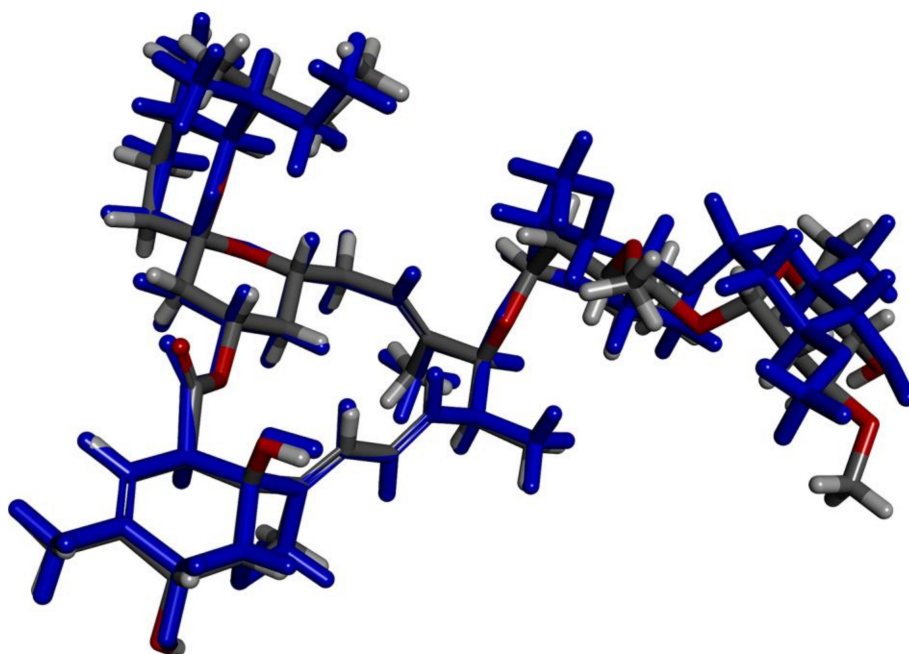


**Figure 3.** Overlay of IVM molecules present in crystal I as determined in the crystal structure (colored by elements) and after in vacuo geometry optimization (blue).

As seen from the figure, the molecular conformation in the free state is close to the one in the crystals. Main differences are associated with the presence of intramolecular hydrogen bonds of the OH $\cdots$ O type, which are formed in vacuo between the hydroxy groups present in the molecule, whilst, in the crystals, these groups are involved in intermolecular hydrogen bonds. The geometrical parameters of these bonds are as follows: angle O39–H39 $\cdots$ O1 is equal to 113.5°, H39 $\cdots$ O1 length is 2.146 Å; O37–H37 $\cdots$ O23 is 144.9°, H37 $\cdots$ O23 is 1.865 Å; O57–H57 $\cdots$ O58 is 111.5° and H57 $\cdots$ O58 is 2.278 Å. Table S2 (Supporting Information) lists the values of selected torsion angles; for these angles, a difference is observed in the free state and in the crystal structure.

As already mentioned, the hydroxy groups form intermolecular hydrogen bonds in the crystal structure. The hydroxy group O39–H39 forms a moderate hydrogen bond O39–H39 $\cdots$ O58 ( $-1 + x, 1 + y, z$ ) with length 3.048(7) Å (H39 $\cdots$ O58 = 2.14 Å, O39–H39 $\cdots$ O58 = 178°). The hydroxy group O57–H57 forms bifurcated hydrogen bonds O57–H57 $\cdots$ O37 ( $1+x, y, z$ ) (O57 $\cdots$ O37 = 2.856(6) Å, H57 $\cdots$ O37 = 2.35 Å, O57–H57 $\cdots$ O37 = 121°) and O57–H57 $\cdots$ O23 ( $1+x, y, z$ ) (O57 $\cdots$ O23 = 3.024(6) Å, H57 $\cdots$ O23 = 2.25 Å, O57–H57 $\cdots$ O23 = 158°). Hydrogen bond C61–H61c $\cdots$ O39 ( $-x, -1+y, 1-z$ ), which can be considered a moderate hydrogen bond of the CH $\cdots$ O type, should be also noted. The parameters of this bond are as follows: C61 $\cdots$ O39 = 3.263(7) Å, H61c $\cdots$ O39 = 2.80 Å and C61–H61c $\cdots$ O39 = 110°. By means of these intermolecular hydrogen bonds, three-dimensional framework containing voids is formed from IVM molecules. Figure 4 shows a projection of the unit cell of crystal I along the monoclinic axis. For geometric modeling of voids in crystals, solvents were removed formally and volumes of voids were then calculated. As it can be seen, there are two types of the voids: one of them lies in special positions (on symmetry axes of order 2), its volume is 82 Å<sup>3</sup>; the second void with volume of 221 Å<sup>3</sup> corresponds to general positions.

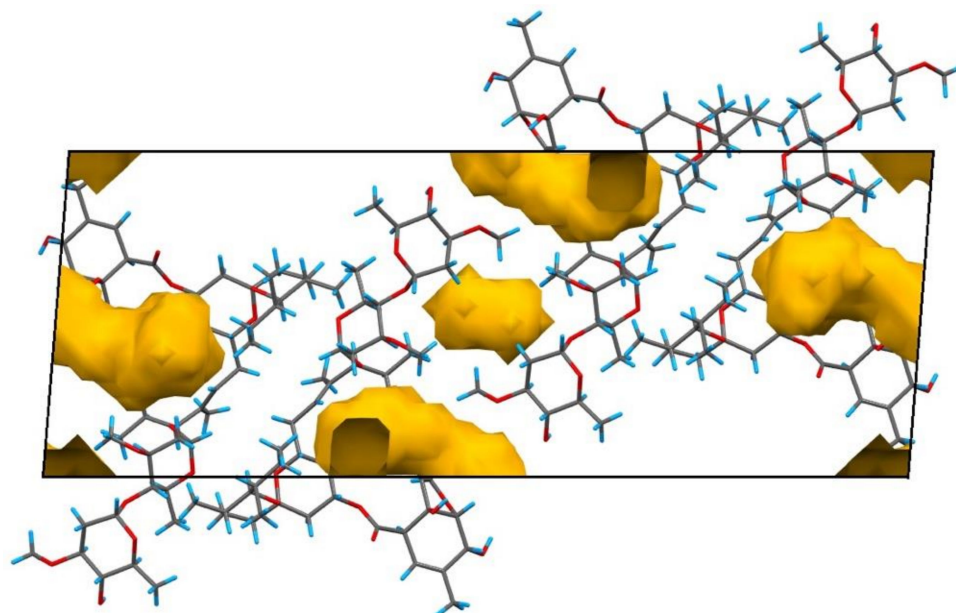


**Figure 4.** A projection of the unit cell of crystal I along the monoclinic axis showing the voids.

It is known that many molecules of macrocyclic compounds are characterized by the fact that the function of distribution of the electrostatic potential has considerable extrema [39]; this allows the molecules to form supramolecular adducts with ions and polar molecules. However, for the IVM molecule, the electrostatic potential obtained from the DFT calculation of the distribution of electron density does not contain significant extrema. This is also the case for other macrocyclic molecules [40]. For this reason, molecules of IVM can form inclusion compounds with polar molecules due to the formation of hydrogen bonds.

Disordered ethanol molecules fill the larger voids in the crystal structure and form hydrogen bonds of the OH $\cdots$ O type with oxygen atom O57. This oxygen atom and carbon, which is attached to O57 atom, were located from a differential Fourier synthesis and refined with  $g = 1.0$ . However, the methyl group of ethanol is disordered, and two carbon atoms of this group were located with a differential synthesis and refined with  $g = 0.5$ . The length of this hydrogen bond is 2.832(9) Å. The smaller voids are filled with disordered water molecules, which form hydrogen bonds with the lengths of 2.67(1)–3.12(1) Å. It should be noted that this crystal structure is isomorphous to the structure of avermectin B<sub>1a</sub>, in which the voids are filled with methanol molecules [21].

The crystal structure of solvate **I** is isomorphous to the structure of IVM-acetone-chloroform solvate (refcode BIFYOF in the Cambridge Crystallographic Database). The void that is occupied by chloroform molecules in BIFYOF in crystal **I** is filled with disordered water molecules. That is why the cell volume is by 96.3 Å<sup>3</sup> lower than that of the BIFYOF structure.

We were interested in testing whether IVM can be crystallized with solvent molecules exceeding the size of the voids (see Figure 4). It turned out that, upon crystallization of IVM from GVL, IVM forms molecular crystals **II** of orthorhombic system (space group  $P2_12_12_1$ ) with two independent molecules of IVM in the asymmetric unit. For both molecules, the occupancy  $g$ -factor of IVM B<sub>1a</sub> is 0.8. IVM molecules form a three-dimensional framework by means of a system of intermolecular hydrogen bonds. This framework also contains voids; Figure 5 gives a projection of the unit cell along the crystallographic parameter  $a$  showing their layout. The volume of voids is 552 Å<sup>3</sup>, and they are filled with GVL molecules. Figure 6 shows a content of the asymmetric unit of the crystal. The value of occupation  $g$ -factor for the solvent is 0.5; this means that not all voids are filled with GVL. It should be noted that, in the crystal structure, there molecules of (*R*)-enantiomer of GVL are present despite the fact that a racemic solvent was used for the crystallization. This suggests that IVM is suitable for the separation of racemic solvents.

The conformation changes of the IVM molecule in solvate **II** are small, but the system of hydrogen bonds in the crystal structure differs from solvate **I**. The strongest intermolecular hydrogen bonds that form the framework are as follows: O57I–H $\cdots$ O43II ( $-1/2 + x, 3/2 - y, 1 - z$ ) with length 2.904(5)Å (H $\cdots$ O = 2.01 Å, O–H $\cdots$ O = 159°); O37II–H $\cdots$ O57I ( $x, y, z$ ) with length 2.694(5)Å (H $\cdots$ O = 1.82 Å, O–H $\cdots$ O = 166°) and O57II–H $\cdots$ O43I ( $1 - x, 1/2 + y, 1/2 - z$ ) with length 2.869(5)Å (H $\cdots$ O = 2.11 Å, O–H $\cdots$ O = 154°), where I and II are the designations of the independent molecules. Among the weak hydrogen bonds, the contact O37I–H $\cdots$ O1s ( $x, y, z$ ) (O $\cdots$ O = 2.494(9) Å, H $\cdots$ O = 2.99Å, O–H $\cdots$ O = 122°) that binds the IVM molecule with the solvent (GVL) should be distinguished.

In continuation of the study, crystallization of IVM from MTBE solution was also carried out. The size of the molecule of the solvent (MTBE) is relatively large and approaches the size of GVL. It turns out that IVM crystallizes in orthorhombic system and forms crystal structure **III** that is isomorphous to crystal structure **II** with  $g = 0.8$  for the B<sub>1a</sub> component of IVM. The voids of crystal structure **III** are filled with disordered MTBE molecules.

Conformation of IVM in both isomorphous monoclinic structures (**I** and BIFYOF) and conformation of each symmetrically unique molecule in both orthorhombic structures (**II** and **III**) are identical, as shown in Figures S1–S3 (Supplementary Materials). Meanwhile, conformation of IVM present in monoclinic structures and in orthorhombic structures is different (see Figure 7). The conformation of IVM in monoclinic structures is the most differing, while the conformation for both symmetrically independent molecules in orthorhombic structures are also notably different.

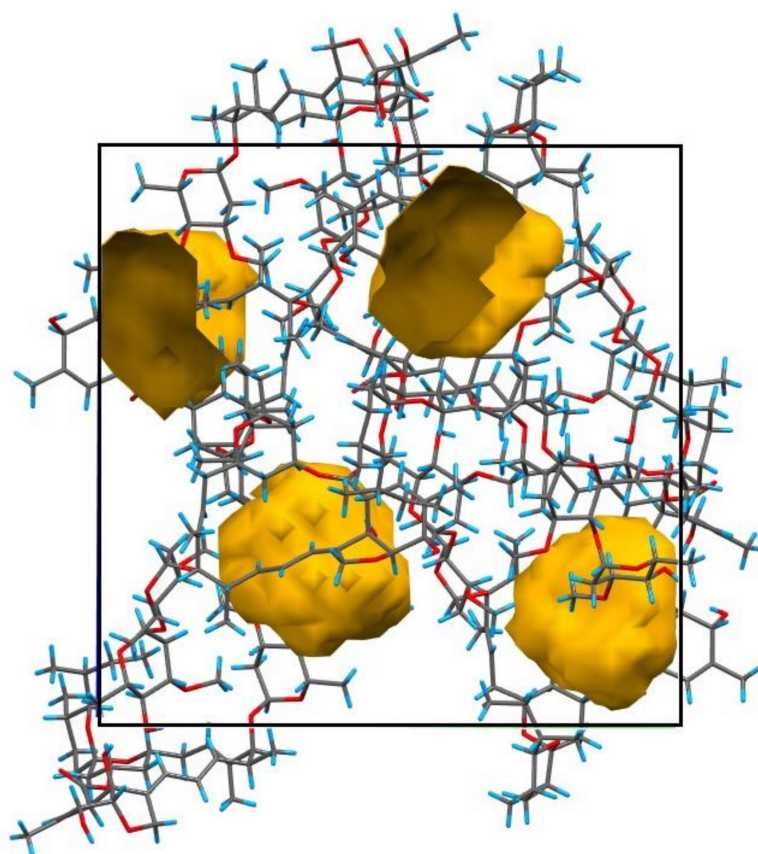


**Figure 5.** A projection of the unit cell of crystal **II** on the crystallographic plane (100) showing the voids.

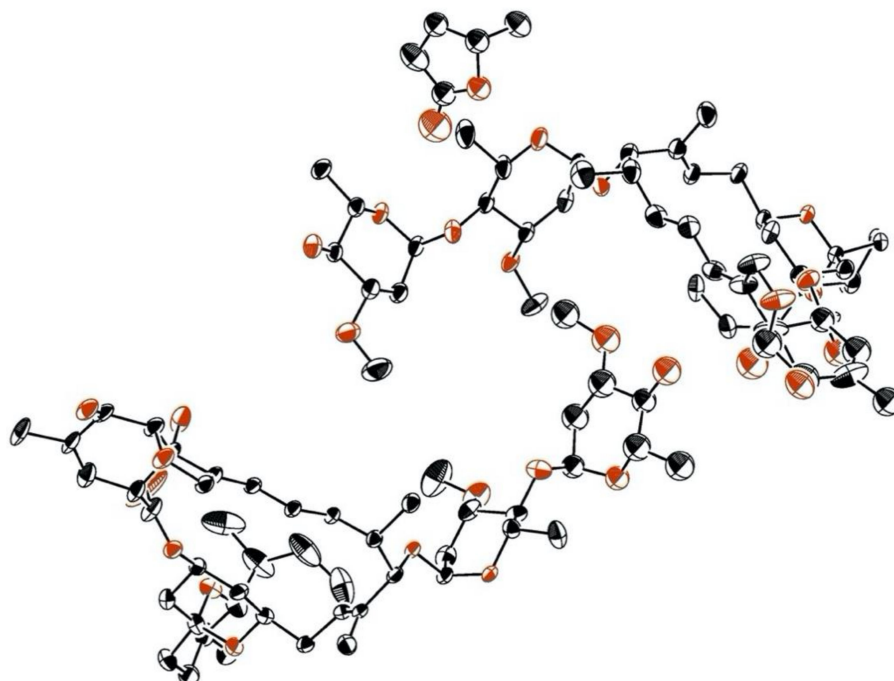


**Figure 6.** ORTEP diagram of two independent molecules of IVM in the asymmetric unit of crystal **II** showing thermal ellipsoids with a 50% probability level. For the sake of clarity, hydrogen atoms and solvent have been omitted.

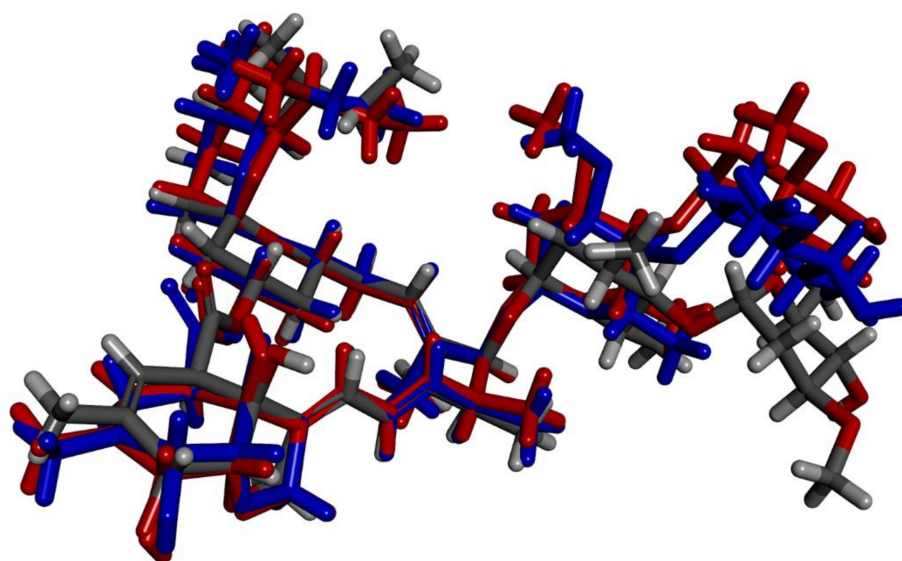


**Figure 7.** Overlay of IVM molecules present in crystal **I** (colored by elements, representing conformation in monoclinic structures; overlay of conformation in **I** and BIFYOF is given in Figure S1, Supplementary Materials) and crystal **II** (blue and red, representing conformation in orthorhombic structures, overlays of conformations in **II** and **III** are given in Figures S2 and S3, (Supplementary Materials).

### 3.2. Qualitative Analysis of Intermolecular Interactions: Hirshfeld Surface and 2D Fingerprint Plots

Crystal structures of IVM solid forms were also analyzed using Hirshfeld surfaces. This, however, was complicated by the fact that part of the structures contained disordered solvent molecules and the fact that all three of them were actually solid solutions. Therefore, ethanol molecules in one of its potential position was used for IVM ethanol solvate **I** in this analysis. Hydrogen atoms were added to the solvent molecule in IVM MTBE solvate **III** in Mercury 2020.2.0. Two hydrogen atoms were removed from the acetone molecule in BIFYOF to obtain molecule with reliable atom arrangement. In all structures of **I**, **II** and **III**, only the geometry corresponding to  $B_{1a}$  ( $R = Et$ ) was used.

The Hirshfeld surfaces of IVM molecule in the analyzed structures are given in Figure 8 (both sides of the molecule are shown). It can be seen that, as expected, the closest normalized distances between the atoms involved in intermolecular interactions are present for the atoms that form conventional and also weak hydrogen bonds (most obviously, hydroxy groups containing oxygen atoms O37, O39 and O57, carbonyl group oxygen atom O23 and part of the ether-type oxygen atoms). As could be expected, Hirshfeld surfaces of both monoclinic structures were quite similar and exhibited more pronounced difference if compared to the surfaces of IVM in orthorhombic structures. Meanwhile, Hirshfeld surfaces of both symmetrically independent molecules of the orthorhombic structures also demonstrated notable differences showing that each of the molecule forms different intermolecular interactions. These differences can be partially associated with the different conformation of the molecules in monoclinic and orthorhombic structures and each symmetrically independent molecule in orthorhombic structures.

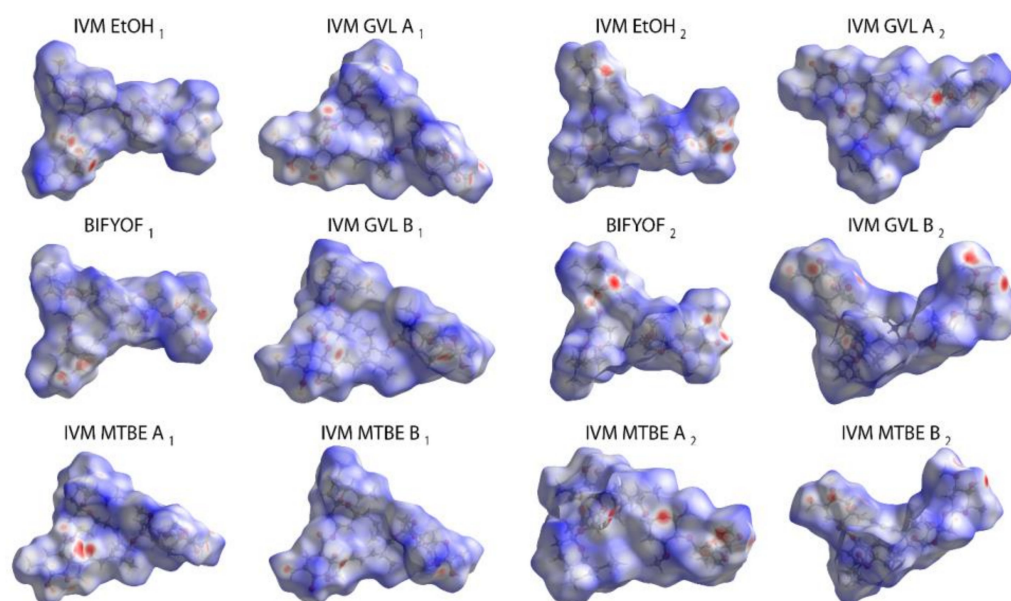


**Figure 8.** Hirshfeld surfaces of IVM in the analyzed structures. All surfaces designated by 1 (on the left) correspond to front view, whereas surfaces designated by 2 (on the right) correspond to the back view. A and B designates each of symmetrically independent molecules.

Two-dimensional fingerprint plots of these Hirshfeld surfaces are given in Figure 9. Again, it can be seen that plots obtained from monoclinic structures are highly similar and there are differences to the plots obtained from the orthorhombic structures, most notably, in the points representing  $H \cdots O$  contacts, showing that there are shorter contacts present in the monoclinic structures. Meanwhile, the differences between plots for both symmetrically independent molecules of orthorhombic structures are notably less pronounced with the most notable difference again being the arrangement of points representing  $H \cdots O$  contacts and illustrating that both symmetrically independent molecules form hydrogen bonds of different geometric parameters.

Summary of the quantitative analysis of the contact types present in the Hirshfeld surfaces is given in Figure 10. Using this representation, it can be seen that there were no major differences in the relative contribution of different contact types in Hirshfeld surfaces of IVM structures. In solvate BIFYOF containing acetone and chloroform as solvents, part of the  $H \cdots H$  contacts were replaced with  $H \cdots Cl$ , but the sum of these two contact types was the same as for purely  $H \cdots H$  contacts for the remaining surfaces. The most notable difference among all surfaces seemed to be the larger number of  $H \cdots O$  contacts present on the surface of A molecule II.

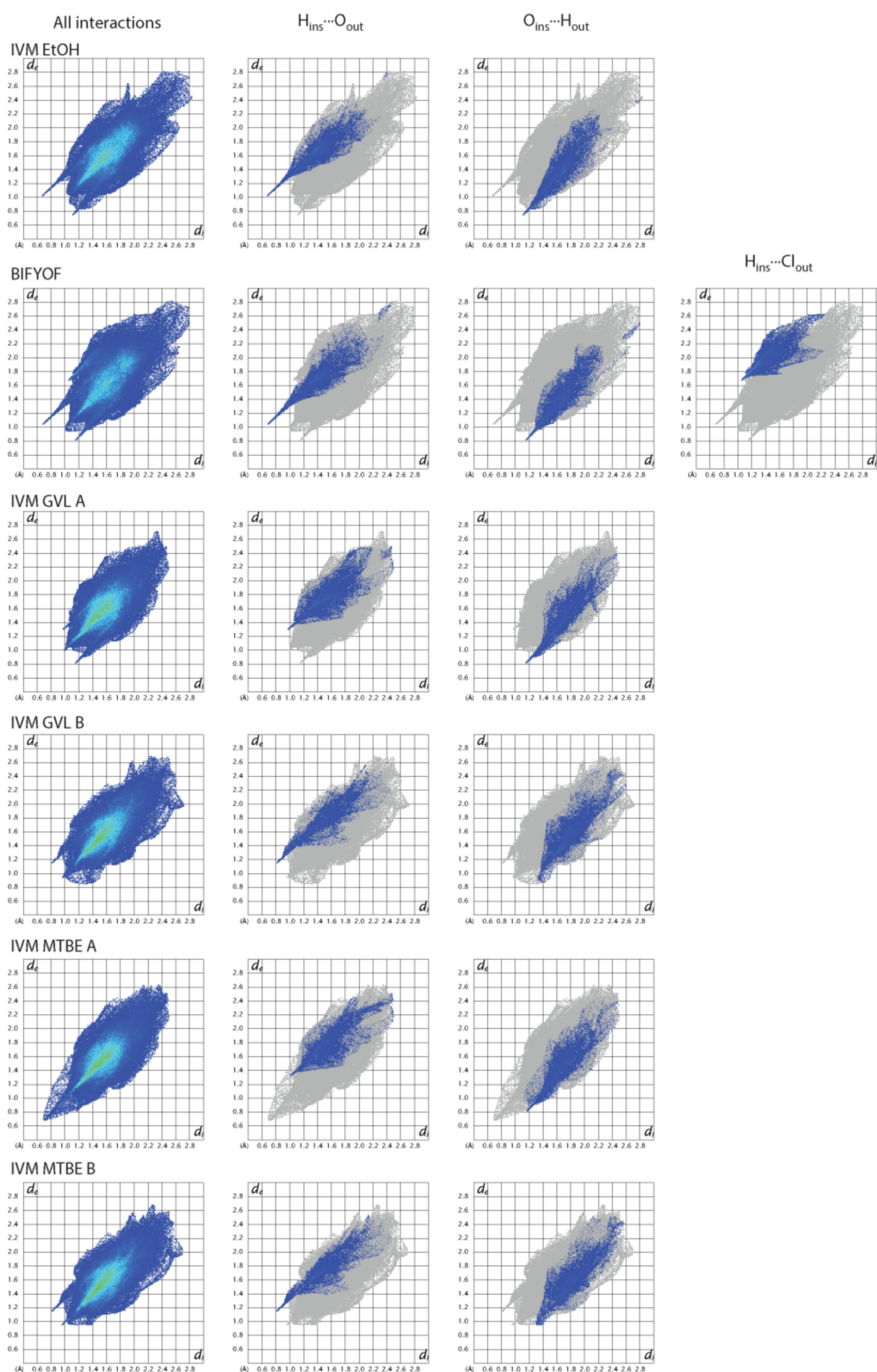


**Figure 9.** Two-dimensional fingerprint plots of Hirshfeld surfaces of IVM structures showing the regions associated with the types of interatomic contacts  $H \cdots O$ ,  $O \cdots H$  and  $H \cdots Cl$  (present only in the structure BIFYOF).

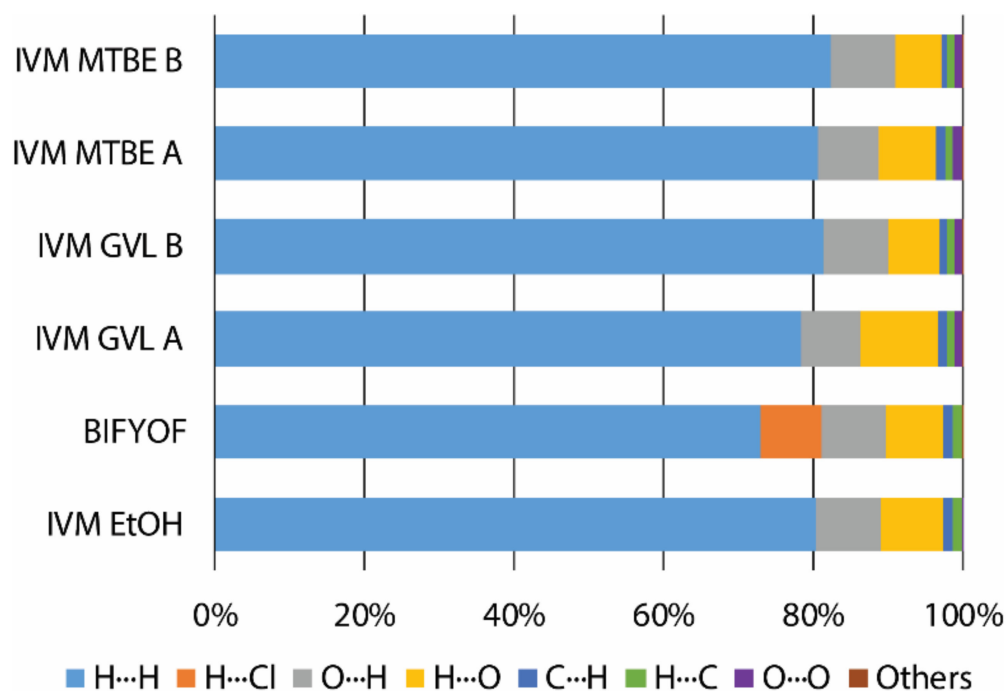


**Figure 10.** Percentage contributions of individual contacts to the Hirshfeld surface area for the analyzed IVM crystal structures.

### 3.3. Intermolecular Interaction Energy of IVM Ethanol Solvate I

In order to get an additional quantitative picture of the intermolecular interactions of the crystal structure of solvate I, calculation of interaction energies was performed in CrystalExplorer17 by assessing the electrostatic ( $E_{\text{ele}}$ ), polarization ( $E_{\text{pol}}$ ), dispersion ( $E_{\text{dis}}$ ) and exchange-repulsion ( $E_{\text{rep}}$ ) terms that together form the total interaction energy ( $E_{\text{tot}}$ ) (see Table 2) [36,41]. However, as water molecules exhibit partial occupancy factors and are not a critical part of the hydrogen bonding network, they were excluded from the structure prior to these calculations.

As can be seen from Table 2, the greatest contribution to stabilization of this structure is made by the interactions between neighboring IVM molecules and, in most cases, these interactions are dominated by dispersion energy component. Additionally, even for the hydrogen-bonded molecule pairs the dispersion energy component is dominant or comparable to the electrostatic components (the highest importance of electrostatic components is observed in a pair having  $E_{\text{ele}} = -43.3 \text{ kJ mol}^{-1}$ ,  $E_{\text{pol}} = -13.6 \text{ kJ mol}^{-1}$  and  $E_{\text{disp}} = -56.2 \text{ kJ mol}^{-1}$ ). This can be easily understood considering the size of the molecule and the relatively small amount of hydrogen bonds present in this structure (compared to the weak and dispersion interactions). Notably lower contribution in the stabilization of this IVM crystal structure is provided by interaction between IVM and ethanol molecules, and even here electrostatic interactions and dispersion interactions provide similar contribution, and only in the pair connected by a hydrogen bond the electrostatic components are the dominant ones.

It follows from the calculations that the energy of the crystal lattice consists mainly of the energies of interactions between IVM molecules, which form the framework of the structure. This means that substance I is an exemplary compound of the host-guest type. In this crystal structure, the voids can be filled with molecules of other solvents if the size of these solvent molecules corresponds to these voids. This is observed in the crystal structure of BIFYOF, where the structure and symmetry of the IVM framework are preserved.

**Table 2.** The pairwise total interaction energy ( $E_{\text{tot}}$ ) and its components (electrostatic ( $E_{\text{ele}}$ ), polarization ( $E_{\text{pol}}$ ), dispersion ( $E_{\text{dis}}$ ) and exchange-repulsion ( $E_{\text{rep}}$ ) energy terms) for the closest molecule pairs (having atoms within 3.8 Å radius from the central molecule) for IVM-ethanol solvate I calculated in CrystalExplorer17.

Symmetry	R/Å	$E_{\text{ele}}$ kJ/mol	$E_{\text{pol}}$ kJ/mol	$E_{\text{dis}}$ kJ/mol	$E_{\text{rep}}$ kJ/mol	$E_{\text{tot}}$ kJ/mol	Contact <sup>1</sup>
x, y, z	9.18	−4.4	−1.7	−46.8	23.4	−32.3	IVM-IVM
−x + 1/2, y + 1/2, −z + 1/2	10.42	−12.5	−1.9	−87.1	50.1	−59.5	IVM-IVM
−x + 1/2, y + 1/2, −z + 1/2	17.43	−3.3	−0.4	−18.5	10.4	−13.4	IVM-IVM
x, y, z	14.82	−43.3	−13.6	−56.2	57	−69.6	IVM-IVM HBS
−x, y, −z	11.35	−8.8	−4.6	−77.2	62.4	−41.3	IVM-IVM
−x, y, −z	14.60	−5	−1.4	−8.7	4.1	−11.5	IVM-IVM
−x, y, −z	22.32	0	−0.1	−6.3	3.2	−3.6	IVM-IVM
-	2.65	−14.5	−3	−40.6	27.9	−35.7	IVM-EtOH
x, y, z	17.43	−1	−4.3	−47.9	29.7	−27.7	IVM-IVM
-	7.28	−1.7	−0.6	−13.3	7.7	−9.1	IVM-EtOH
-	12.39	0.5	−0.1	−1.9	0.1	−1.2	IVM-EtOH
−x, y, −z	14.10	−0.6	−0.8	−22	3.8	−18	IVM-IVM
-	13.5	−35.4	−7.8	−12.2	37.8	−30.5	IVM-EtOH HB
-	14.9	−1.1	−0.1	−2.9	1.6	−2.8	IVM-EtOH

<sup>1</sup> IVM-IVM denotes that this is an interaction between two IVM molecules, while IVM-EtOH is an interaction between IVM and ethanol. HB and HBS indicate that there are one or multiple hydrogen bonds connecting the respective molecules.

#### 4. Conclusions

In summary, three new pseudopolymorphs of IVM were prepared: **I** as the ethanol solvate, **II** as the GVL solvate and **III** as the MTBE solvate. In all cases, crystallization of the commercially available IVM provided a solid solution of two components  $B_{1a}$  and  $B_{1b}$  with the retaining of the natural 80:20 ratio.

The major feature of the molecular structure is the *crown*-conformation of the main macrocyclic ring. Propensity of IVM to crystallize together with solvent molecules is associated with the molecule being bulky and, as other similar compounds, IVM cannot pack efficiently without leaving voids in the crystal structure, which are filled with solvent molecules. In a solvent with relatively small molecules (ethanol), IVM forms monoclinic crystal structure (space group  $I2$ ), which contains two types of voids with volumes of 82 and 221 Å<sup>3</sup>. The largest void contains one disordered solvent molecule, while the small one contains disordered water molecules. When crystallized from solvents with larger molecules (GVL and MTBE), IVM forms orthorhombic crystal structure (space group  $P2_12_12_1$ ). In case of solvates **II** and **III**, only one type of void is formed with a much bigger volume: 552 Å<sup>3</sup>.

Conformation of IVM found in crystals is generally retained through all obtained forms **I**, **II** and **III** and also in solvate BIFYOF, data for which has been previously deposited in the Cambridge Crystallographic Data Centre. Conformation determined for a molecule, modeled by DFT calculations, is near to the conformation found in crystals. The Hirshfeld surface analysis indicated the dominant role of dispersive contacts for H···H (80% on average), O···H (10% on average) and H···O (10% on average).

The energy of crystal lattice was calculated for model crystal system **I**, which contains IVM molecule and one ethanol molecule. The interaction between IVM molecules themselves provides the biggest contribution to the crystal energy. By means of these interactions between IVM molecules, the molecular framework in the crystal structure is formed.

Thermal analysis shows wide peaks in DSC patterns, typical for solid solutions see Figures S4 and S5 (Supplementary Materials). The peak of the melting process is observed at 165 °C for pseudopolymorph **I** and at 172 °C for **II**. Additionally, the thermal analysis

data show that, in solvate **II**, the substance loses the solvent (GVL) at 83 °C. In crystal **I**, this process is not observed.

**Supplementary Materials:** The following are available online at <https://www.mdpi.com/2073-4352/11/2/172/s1>, Table S1: Atomic Cartesian coordinates for IVM B<sub>1a</sub> from DFT, Table S2: Selected torsion angles for **I**, Figure S1: Overlay of IVM molecules present in **I** and BIFYOF, Figure S2: Overlay of the first kind of symmetrically unique IVM molecules present in **II** and **III**, Figure S3: Overlay of the second kind of symmetrically unique IVM molecules present in **II** and **III**, Figure S4: Processed DSC and TGA data for **I**, Figure S5: Processed DSC and TGA data for **II**.

**Author Contributions:** K.S. conceived and designed the experiments, conceptualized the work and prepared the manuscript for publication; A.B. provided crystal structure analysis, reviewed and edited the manuscript; S.B. provided acquisition of funding and supervision of the research, conducted the X-ray analysis, reviewed and edited the manuscript. All authors discussed the contents of the manuscript. All authors have read and agreed to the published version of the manuscript.

**Funding:** This research was funded by project “Development of innovative face cosmetics with controlled release of active ingredients by use of Metal Organic Frameworks or Cocrystals” (ERAF project number 1.1.1.1/18/A/176).

**Conflicts of Interest:** The authors declare no conflict of interest.

## References

1. Campbell, W.; Fisher, M.; Stapley, E.; Albers-Schonberg, G.; Jacob, T. Ivermectin: A potent new antiparasitic agent. *Science* **1983**, *221*, 823–828. [[CrossRef](#)] [[PubMed](#)]
2. Crump, A. Ivermectin: Enigmatic multifaceted ‘wonder’ drug continues to surprise and exceed expectations. *J. Antibiot.* **2017**, *70*, 495–505. [[CrossRef](#)]
3. Ashour, D.S. Ivermectin: From theory to clinical application. *Int. J. Antimicrob. Agents* **2019**, *54*, 134–142. [[CrossRef](#)]
4. Laing, R.; Gillan, V.; Devaney, E. Ivermectin—Old Drug, New Tricks? *Trends Parasitol.* **2017**, *33*, 463–472. [[CrossRef](#)]
5. Perez-Garcia, L.A.; Mejias-Carpio, I.E.; Delgado-Noguera, L.A.; Manzanarez-Motezuma, J.P.; Escalona-Rodriguez, M.A.; Sordillo, E.M.; Mogollon-Rodriguez, E.A.; Hernandez-Pereira, C.E.; Marquez-Colmenarez, M.C.; Paniz-Mondolfi, A.E. Ivermectin: Repurposing a multipurpose drug for Venezuela’s humanitarian crisis. *Int. J. Antimicrob. Agents* **2020**, *56*, 106037. [[CrossRef](#)] [[PubMed](#)]
6. Juarez, M.; Schcolnik-Cabrera, A.; Dueñas-Gonzalez, A. The multitargeted drug ivermectin: From an antiparasitic agent to a repositioned cancer drug. *Am. J. Cancer Res.* **2018**, *8*, 317–331.
7. Laudisi, F.; Marònek, M.; Di Grazia, A.; Monteleone, G.; Stolfi, C. Repositioning of Anthelmintic Drugs for the Treatment of Cancers of the Digestive System. *IJMS* **2020**, *21*, 4957. [[CrossRef](#)]
8. Mudassar, F.; Shen, H.; O’Neill, G.; Hau, E. Targeting tumor hypoxia and mitochondrial metabolism with anti-parasitic drugs to improve radiation response in high-grade gliomas. *J. Exp. Clin. Cancer Res.* **2020**, *39*, 208. [[CrossRef](#)] [[PubMed](#)]
9. Tang, M.; Hu, X.; Wang, Y.; Yao, X.; Zhang, W.; Yu, C.; Cheng, F.; Li, J.; Fang, Q. Ivermectin, a potential anticancer drug derived from an antiparasitic drug. *Pharmacol. Res.* **2020**, 105207. [[CrossRef](#)]
10. Sahni, D.R.; Feldman, S.R.; Taylor, S.L. Ivermectin 1% (CD5024) for the treatment of rosacea. *Expert Opin. Pharmacother.* **2018**, *19*, 511–516. [[CrossRef](#)]
11. McGregor, S.P.; Alinia, H.; Snyder, A.; Tuchayi, S.M.; Fleischer, A.; Feldman, S.R. A Review of the Current Modalities for the Treatment of Papulopustular Rosacea. *Dermatol. Clin.* **2018**, *36*, 135–150. [[CrossRef](#)]
12. Feaster, B.; Cline, A.; Feldman, S.R.; Taylor, S. Clinical effectiveness of novel rosacea therapies. *Curr. Opin. Pharmacol.* **2019**, *46*, 14–18. [[CrossRef](#)]
13. Heidary, F.; Gharebaghi, R. Ivermectin: A systematic review from antiviral effects to COVID-19 complementary regimen. *J. Antibiot.* **2020**, *73*, 593–602. [[CrossRef](#)] [[PubMed](#)]
14. Jans, D.A.; Wagstaff, K.M. Ivermectin as a Broad-Spectrum Host-Directed Antiviral: The Real Deal? *Cells* **2020**, *9*, 2100. [[CrossRef](#)]
15. Sen Gupta, P.S.; Rana, M.K. Ivermectin, Famotidine, and Doxycycline: A Suggested Combinatorial Therapeutic for the Treatment of COVID-19. *Acs Pharmacol. Transl. Sci.* **2020**, *3*, 1037–1038. [[CrossRef](#)]
16. Rajter, J.C.; Sherman, M.S.; Fatteh, N.; Vogel, F.; Sacks, J.; Rajter, J.-J. ICON (Ivermectin in COvid Nineteen) study: Use of Ivermectin is Associated with Lower Mortality in Hospitalized Patients with COVID19; Public and Global Health. 2020. Available online: <https://www.medrxiv.org/content/10.1101/2020.06.06.20124461v2> (accessed on 2 February 2021).
17. Gupta, D.; Sahoo, A.K.; Singh, A. Ivermectin: Potential candidate for the treatment of Covid 19. *Braz. J. Infect. Dis.* **2020**, *24*, 369–371. [[CrossRef](#)]
18. Healy, A.M.; Worku, Z.A.; Kumar, D.; Madi, A.M. Pharmaceutical solvates, hydrates and amorphous forms: A special emphasis on cocrystals. *Adv. Drug Deliv. Rev.* **2017**, *117*, 25–46. [[CrossRef](#)] [[PubMed](#)]

19. Pindelska, E.; Sokal, A.; Kolodziejski, W. Pharmaceutical cocrystals, salts and polymorphs: Advanced characterization techniques. *Adv. Drug Deliv. Rev.* **2017**, *117*, 111–146. [CrossRef]
20. Calvo, N.L.; Maggio, R.M.; Kaufman, T.S. Chemometrics-assisted solid-state characterization of pharmaceutically relevant materials. Polymorphic substances. *J. Pharm. Biomed. Anal.* **2018**, *147*, 518–537. [CrossRef] [PubMed]
21. Springer, J.P.; Arison, B.H.; Hirshfield, J.M.; Hoogsteen, K. The absolute stereochemistry and conformation of avermectin B2a aglycone and avermectin B1a. *J. Am. Chem. Soc.* **1981**, *103*, 4221–4224. [CrossRef]
22. Keates, A.C. CCDC 1904192: Experimental Crystal Structure Determination 2019. Available online: <https://www.ccdc.cam.ac.uk/structures/Search?Ccdcid=1904192&DatabaseToSearch=Published> (accessed on 3 February 2021).
23. Jelínková, I.; Vávra, V.; Jindrichova, M.; Obsil, T.; Zemkova, H.W.; Zemkova, H.; Stojilkovic, S.S. Identification of P2X4 receptor transmembrane residues contributing to channel gating and interaction with ivermectin. *Pflug. Arch. Eur. J. Physiol.* **2008**, *456*, 939–950. [CrossRef]
24. Huang, X.; Chen, H.; Shaffer, P.L. Crystal Structures of Human GlyR $\alpha$ 3 Bound to Ivermectin. *Structure* **2017**, *25*, 945–950.e2. [CrossRef] [PubMed]
25. Grobler, M.L.J. Genome-Wide Analysis of Wolbachia-Host Interactions. Master's Thesis, North-West University, Potchefstroom, South Africa, 2000.
26. Rolim, L.A.; dos Santos, F.C.M.; Chaves, L.L.; Gonçalves, M.L.C.M.; Freitas-Neto, J.L.; da Silva do Nascimento, A.L.; Soares-Sobrinho, J.L.; de Albuquerque, M.M.; do Carmo Alves de Lima, M.; Rolim-Neto, P.J. Preformulation study of ivermectin raw material. *J. Anal. Calorim.* **2015**, *120*, 807–816. [CrossRef]
27. Starkloff, W.J.; Bucalá, V.; Palma, S.D.; Gonzalez Vidal, N.L. Design and in vitro characterization of ivermectin nanocrystals liquid formulation based on a top-down approach. *Pharm. Dev. Technol.* **2017**, *22*, 809–817. [CrossRef] [PubMed]
28. Lu, M.; Xiong, D.; Sun, W.; Yu, T.; Hu, Z.; Ding, J.; Cai, Y.; Yang, S.; Pan, B. Sustained release ivermectin-loaded solid lipid dispersion for subcutaneous delivery: In vitro and in vivo evaluation. *Drug Deliv.* **2017**, *24*, 622–631. [CrossRef]
29. Seppala, E.; Kolehmainen, E.; Osmialowski, B.; Gawinecki, R. CCDC 187337: Experimental Crystal Structure Determination 2005. Available online: <https://www.ccdc.cam.ac.uk/structures/Search?Ccdcid=187337&DatabaseToSearch=Published> (accessed on 3 February 2021).
30. Sheldrick, G.M. SHELXT—Integrated space-group and crystal-structure determination. *Acta Cryst. A Found. Adv.* **2015**, *71*, 3–8. [CrossRef]
31. Sheldrick, G.M. A short history of SHELX. *Acta Cryst. A Found. Cryst.* **2008**, *64*, 112–122. [CrossRef]
32. Dolomanov, O.V.; Bourhis, L.J.; Gildea, R.J.; Howard, J.A.K.; Puschmann, H. OLEX2: A complete structure solution, refinement and analysis program. *J. Appl. Cryst.* **2009**, *42*, 339–341. [CrossRef]
33. Turner, M.J.; McKinnon, J.J.; Wolff, S.K.; Grimwood, D.J.; Spackman, P.R.; Jayatilaka, D.; Spackman, M.A. *CrystalExplorer17*; The University of Western Australia: Perth, WA, Australia, 2017.
34. McKinnon, J.J.; Jayatilaka, D.; Spackman, M.A. Towards quantitative analysis of intermolecular interactions with Hirshfeld surfaces. *Chem. Commun.* **2007**, 3814. [CrossRef]
35. Spackman, M.A.; Jayatilaka, D. Hirshfeld surface analysis. *CrystEngComm* **2009**, *11*, 19–32. [CrossRef]
36. Mackenzie, C.F.; Spackman, P.R.; Jayatilaka, D.; Spackman, M.A. *CrystalExplorer* model energies and energy frameworks: Extension to metal coordination compounds, organic salts, solvates and open-shell systems. *IUCr* **2017**, *4*, 575–587. [CrossRef] [PubMed]
37. Bochevarov, A.D.; Harder, E.; Hughes, T.F.; Greenwood, J.R.; Braden, D.A.; Philipp, D.M.; Rinaldo, D.; Halls, M.D.; Zhang, J.; Friesner, R.A. Jaguar: A high-performance quantum chemistry software program with strengths in life and materials sciences. *Int. J. Quantum Chem.* **2013**, *113*, 2110–2142. [CrossRef]
38. Saršūns, K.; Bērziņš, A.; Reķis, T. Solid Solutions in the Xanthone–Thioxanthone Binary System: How Well Are Similar Molecules Discriminated in the Solid State? *Cryst. Growth Des.* **2020**, *20*, 7997–8004. [CrossRef]
39. Marczenko, K.M.; Mercier, H.P.A.; Schrobilgen, G.J. A Stable Crown Ether Complex with a Noble-Gas Compound. *Angew. Chem. Int. Ed.* **2018**, *57*, 12448–12452. [CrossRef] [PubMed]
40. Popov, I.; Chen, T.-H.; Belyakov, S.; Daugulis, O.; Wheeler, S.E.; Miljanić, O.Š. Macrocyclic Embrace: Encapsulation of Fluoroarenes by *m*-Phenylene Ethynylene Host. *Chem. A Eur. J.* **2015**, *21*, 2750–2754. [CrossRef] [PubMed]
41. Turner, M.J.; Grabowsky, S.; Jayatilaka, D.; Spackman, M.A. Accurate and Efficient Model Energies for Exploring Intermolecular Interactions in Molecular Crystals. *J. Phys. Chem. Lett.* **2014**, *5*, 4249–4255. [CrossRef] [PubMed]